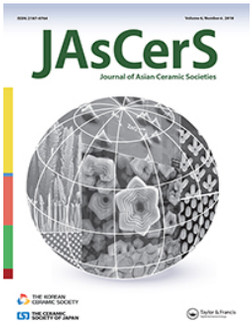

Journal of Asian Ceramic Societies

ISSN: (Print) 2187-0764 (Online) Journal homepage: https://www.tandfonline.com/loi/tace20

Densification of lightweight aluminum borate ceramics by direct sintering of milled powders

M.F. Hernández, G. Suárez, C. Baudin, P. Pena Castro, E.F. Aglietti & N.M. Rendtorff

To cite this article: M.F. Hernández, G. Suárez, C. Baudin, P. Pena Castro, E.F. Aglietti & N.M. Rendtorff (2018) Densification of lightweight aluminum borate ceramics by direct sintering of milled powders, Journal of Asian Ceramic Societies, 6:4, 374-383, DOI: 10.1080/21870764.2018.1539209

To link to this article: https://doi.org/10.1080/21870764.2018.1539209

Published online: 08 Nov 2018.

JOURNAL OF ASIAN CERAMIC SOCIETIES
2018, VOL. 6, NO. 4, 374–383
https://doi.org/10.1080/21870764.2018.1539209

THE CERAMIC SOCIETY OF JAPAN
THE KOREAN CERAMIC SOCIETY
Taylor & Francis
Taylor & Francis Group

FULL LENGTH ARTICLE

OPEN ACCESS
Check for updates

Densification of lightweight aluminum borate ceramics by direct sintering of milled powders

M.F. Hernández[a,b], G. Suárez[a,b,c], C. Baudin[c], P. Pena Castro[c], E.F. Aglietti[a,b] and N.M. Rendtorff[a,b]

[a]Centro de Tecnología de Recursos Minerales y Cerámica (CETMIC): (CIC-CONICET-CCT La Plata), M.B. Gonnet, Argentina; [b]Dpto. de Química, Facultad de Ciencias Exactas, Universidad Nacional de La Plata, La Plata, Argentina; [c]Instituto de Cerámica y Vidrio (ICV), Madrid, España

ABSTRACT

Dense aluminum borate ($Al_{18}B_4O_{33}$) materials were processed by simple milling-sintering of aluminum borate powders obtained by reacting calcined alumina and fine boric acid at temperatures of around 600–800ºC. The effect of milling on the grain size and sintering behavior of the aluminum borate powders was also determined. Sintering began at around 1000°C and was limited by the thermal decomposition (T > 1300 °C) of the borate in to alumina and boron oxide, which volatilize at this temperature. Sub-angular and medium spherical sintered grain microstructures were developed. A hardness of 6 GPa and bulk density below 2.5 g/cm^3 were achieved. The results are accomplished encouraging the structural applications of borate materials.

ARTICLE HISTORY
Received 16 May 2018
Accepted 25 September 2018

KEYWORDS
Aluminum borate; sintering; processing; properties

1. Introduction

The formation of boron-aluminates (BA: $Al_{18}B_4O_{33}$) from alumina and boron oxide occurs at intermediate temperatures (approx 600–800 °C), with respected to other alumina binary systems. These materials present high refractoriness up to 1300ºC, accompanied by chemical inertness in some environments [1]. The chemical and physical properties of boron aluminates are shown in Table 1. The catalytic properties of these phases for some technological reactions is also remarkable [2–4]. Low density in comparison with other similar structural ceramics such as alumina, zircon, zirconia and mullite, is one of the principal merits.

$Al_{18}B_4O_{33}$ materials exhibit a typical whisker or needle morphology (whisker-rod) [5–8]. The utilization of aluminum borate needles or whiskers for reinforcement of aluminum and aluminum-based alloys is the principal application of these phases [9]. Reinforcement of magnesium alloys was proposed as well [10]. Forming composites with metallic elements improves the mechanical behavior of $Al_{18}B_4O_{33}$ as well as its chemical compatibility (low wettability) and microstructural configuration compared with corresponding metallic materials. Vitroceramics with aluminum borates as the crystalline phase were also studied and presented attractive technological properties [11].

As mentioned, refractory and other structural applications were reported, and these were proposed as insulating and filtering materials as well. Besides reaction sintering from alumina and boric oxide [6–8] some other synthetic routes have been proposed and studied. These include: the flux method [5], crystallization from molten salts [12], sol-gel routes and chemical precursors [13–16]. A combustion synthesis route was studied [17] for BA materials as well. Beside alumina, metallic aluminum was also proposed as an aluminum source [18,19].

Furthermore, much attention has been paid to production of whiskers as non-monolithic materials (powders and nano powders) [2–4].

Micro mechanical characterization of the whisker was carried out by Tao et al. [20], who found that it presented outstanding properties, encouraging needle applications.

Orthorhombic boron-aluminate is an important ceramic material for which two slightly different compositions have been assumed: Al_5BO_9 ($5Al_2O_3{\cdot}B_2O_3$) and $Al_{18}B_4O_{33}$ ($9Al_2O_3 \cdot 2B_2O_3$). The formula $Al_{18}B_4O_{33}$ ($\approx Al_{4.91}B_{1.09}O_9$) was derived from the results of chemical analysis when crystal structure data were not yet available. Subsequent structural investigations indicated an actual Al_5BO_9 composition [21]. This was concluded after a complete multitechnique structural characterization.

Several studies have been carried out recently with respect to the incorporation of boron oxide-containing compounds in refractory materials, such as alumina, magnesia and mullite based castables [22–26]. The boron oxide-containing compounds were proposed as effective ceramic mineralizers during thermal treatment of the refractory castables to achieve in situ formation of

CONTACT G. Suárez gsuarez@cetmic.unlp.edu.ar

Table 1. Properties of the aluminum borate $Al_{18}B_4O_{33}$ phase [5].

Property	
Theoretical density (g/cm^3)	2.96
Thermal conductivity (W/m K)	4–6
Young modulus (GPa)	400
Strength (tensile) (MPa)	8000
Hardness (Mohs)	7
Thermal expansion $\times 10^{-6}$ °C^{-1}	≈4.5 (axial) ≈1.9 (radial)

a new crystalline phase with mechanical behavior enhancement. This shows the actual potential of boron-containing materials in the refractory industry.

It is worth pointing out the presumable inherent difficulty of sintering aluminum borate powders based on two facts: their whisker-needle morphology and their thermal decomposition at high temperatures (over 1300 °C). The sintering behavior of aluminum borate powders has not been reported, and in this article we fill this vacancy.

In a recent article [27], we presented a systematic study of the formation of aluminum borate from boric acid and calcined alumina (D_{50}: 2.5 μm). The developed microstructures and properties by a simple milling-pressing-sintering processing route were described. A set of porous ceramic materials was processed and characterized. Both single aluminum borate and alumina – aluminum borate composite materials were obtained. The borate phase presented an interlocking needle morphology which could be assumed to affer good mechanical properties. The sintering difficulty of this phase was established, and based on the needle morphology, the thermal decomposition and the low-temperature volatilization of boron oxide. In a second article, the mechanical behavior was assessed using a diametral compression test. The observed behavior was explained in terms of the microstructural features of the porous needle microstructure. The results encouraged application of these materials as well [27,28], especially in porous applications.

The principal objective of the present article is to obtain densified aluminum borate ceramics and to evaluate some of their technological properties. For this, an aluminum borate powder ($Al_{18}B_4O_{33}$) obtained from a stoichiometric alumina-boric acid mixture fired at 1200° C and subsequently attrition milled was employed as starting powder. The milling procedure and the starting powders properties are firstly described. The thermal and sintering behaviors are then analyzed together with some of the technological properties of the resulting ceramics.

2. Experimental procedure

2.1. Starting powder

The aluminum borate ($Al_{18}B_4O_{33}$) studied was obtained from a thermal reaction of calcined alumina (A2G; Amatis, USA) and commercial boric acid (Borax Argentina SA, Argentina) with 99.8% H_3BO_3, (56.2% B_2O_3), CAS No.: 10043–35–3. The boric acid was dry-milled in a disc and ring mill (Herzog HS-100). The starting powders were milled in isopropyl alcohol and calcined at 1200°C for 60 min with 10°C/min of heating rate.

The obtained powder was attrition milled in a 100 ml jar with 1/3 of the total volume occupied by 1 mm diameter 3 mol% Y_2O_3-stabilized zirconia balls in isopropyl alcohol at 880 rpm.

The particle size evolution with milling time was analyzed by Laser Diffraction Particle Size Distribution Analyzer (Malvern Hydro 2000G, UK); this technique permits particle size distribution analysis in the 0.01–3500 μm range. The starting powder and milled powder were analyzed by X-ray diffraction (XRD PW 3710-, Philips, The Netherlands, with Kα: Cu as incident radiation and Ni filter) in the range 2θ between 10 and 70° in order to evaluate the effect of milling time on crystallinity. The particle shape and morphology were analyzed as well by scanning electron microscopy (SEM-JEOL JMS –6000, Japan).

2.2. Thermal behavior of the milled powder

The thermal behavior of the milled powder was studied by thermogravimetry (TG, Rigaku Evo plus II, Japan), differential thermal analysis (DTA Rigaku Evo plus II, Japan) and dilatometry (TMA Rigaku Evo Plus II, Japan). All the thermal analyses were carried out at a heating rate of 5°C/min in air up to 1400°C.

The crystalline phases at intermediate temperatures (200, 400, 600 and 1200°C) were analyzed in powder samples heated and quenched in an electric furnace in alumina crucibles by X-ray diffraction (XRD) under the same conditions as mentioned above. The same characterization was carried out for the sintered samples.

2.3. Shaping and sintering

The milled powders (180 min) were dried (24 h at 110°C) and sieved (above 63 microns) then die-pressed uniaxially (100 MPa) in to disc-shaped samples with 10 mm diameters and ≈2 mm heights.

The samples were thermally treated in an electric furnace in air with both heating and cooling rates of 5°C/min up to different final temperatures between 1250 and 1500°C and a dwelling time of 120 min. For 1300°C, the soaking time was also explored as a processing variable, with materials fired for 300 and 600 min compared to those treated for 120 min.

2.4. Characterizations of the samples

The materials, characterization were determined by XRD analysis (under the mentioned conditions for

Table 2. Pore structure and b parameter relationships [29].

Pore structure (rice 1996)	b
Cylindrical pores in cubic stacking	1.4
Spherical pores in cubic stacking	3
Solid spheres in cubic stacking	5
Solid spheres in rhombohedral stacking	9

the starting powder). The Archimedes method was employed to evaluate the apparent density and open porosity. The resulting microstructures were analyzed by scanning electron microscopy (FEI Quanta200 20 Kv and electrodispersed electron detector) for both fracture surfaces and surfaces polished with diamond paste (down to 1 μm) as well as chemically etched (HCl 10%, 3 min) and gold-coated surfaces.

Vickers hardness was determined with a 1 kgf load and 10-second dwelling time (Buhler IndentaMet, USA); the average for each material was10 indentations.

The minimum solid area models (MSA) were developed In 1996 by Rice et al. [29]. The experimental values of the determined properties (hardness, stiffness, strength, etc.) were related to the porosity and the pure dense value according to the following exponential relationship (Equation 1):

$$Hv = Hv_0.exp(-b.P) \quad (1)$$

In this case, Hv is the Vickers hardness; Hv_0 is the pure dense value of the hardness and P the pore fraction; and b is a parameter determined by the character of the porosity. This expression has been widely used for porosity studies in the past, first for studies conducted on an empirical basis, and then for studies conducted on an analytical basis for different stacking of spherical particles [29]. The various pore structures studied are listed in Table 2.

Intermediate values can be understood as pore structures corresponding to a combination of each model.

3. Results and discussion

3.1. Aluminum borate attrition milling effect

Figure 1 shows the particle size evolution as a function of time for the $Al_{18}B_4O_{33}$ starting powder. The initial powder exhibited a bimodal distribution centered on ≈35 and 1–2 μm. Some large agglomerates (D ≈ 100 μm) were also detected.

After 60 min, the largest agglomerates disappeared and the 35 μm fraction evolved to smaller particle sizes, with the distribution centered around 10 μm. This change was also accompanied by an important increase in the 1 μm fraction. The smallest detected particle sizes are around twenty times the detection limit (0.01 μm). After 120 min, the maximum particle size is around 2 microns with a small amount approaching an ≈7 μm size fraction.

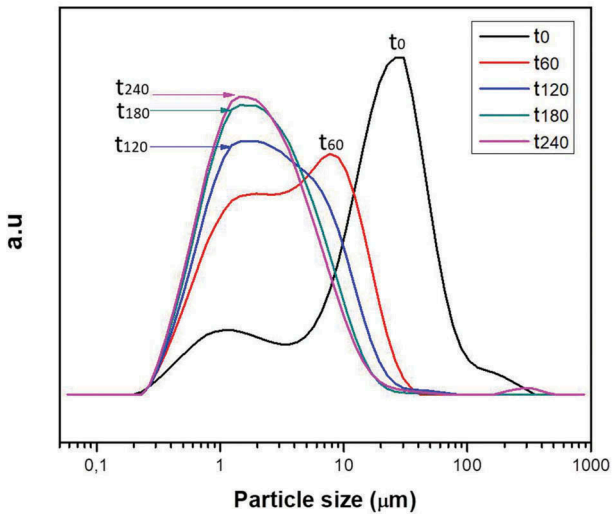

Figure 1. Particle size distribution of the aluminum borate $Al_{18}B_4O_{33}$ starting powder for different attrition milling times.

After 180 min treatment the particle size distribution is apparently monomodal and centered at 2 μm. The distribution can be explained as D_{10} = 0.3; D_{50} = 1.1 and D_{90} = 10 microns.

Further milling treatment (240 min) did not affect the particle size distribution. For this reason, a 180 min milling time was chosen as the optimal milling time for the powder in this sintering study.

Figure 2 shows the XRD patterns of the milled (180 min) and unmilled aluminum borate powder. In both cases the principal peaks of a aluminum borate ($Al_{18}B_4O_{33}$) are observed (PDF: 00-032-0003), accompanied by a small reflection corresponding to the $Al_4B_2O_9$ phase (PDF: 00-029-0010). No important changes in the peak shapes or widths were observed, indicating that the milling process did not affect crystallinity. After milling treatment a small zirconia reflection was observed. This evidences slight contamination by the milling media, and it is assumed that this amount of zirconia contamination does not affect the sintering process.

Figure 3 shows an SEM image of 180 min attrition milled aluminum borate powder. In general, the observed particle size is consistant with the laser scattering results (Figure 1). The initial borate powder consisted of whiskers with a 1 μm diameter and an aspect ratio of over 20 [27]. The milled powder particles exhibited rod shapes with aspect ratios between 1 and 4. The rod extremes are irregular. The observed shapes suggest whisker breakage of the fragile transversal mechanism during milling. No particles below 0.1 μm were detected, which is consistent with the laser scattering results as well.

3.2. TG-DTA

Figure 4 shows the TG-DTA curves of $Al_{18}B_4O_{33}$ powder. Four mass losses can be observed (≤100 °C; ≈337 °

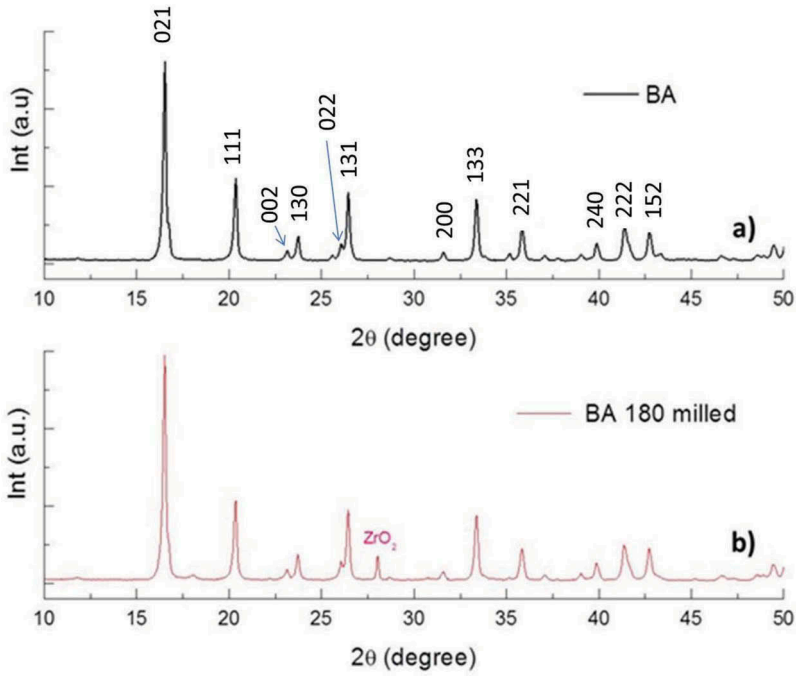

Figure 2. XRD patterns of the un-milled (a) $Al_{18}B_4O_{33}$ and milled (b) powders.

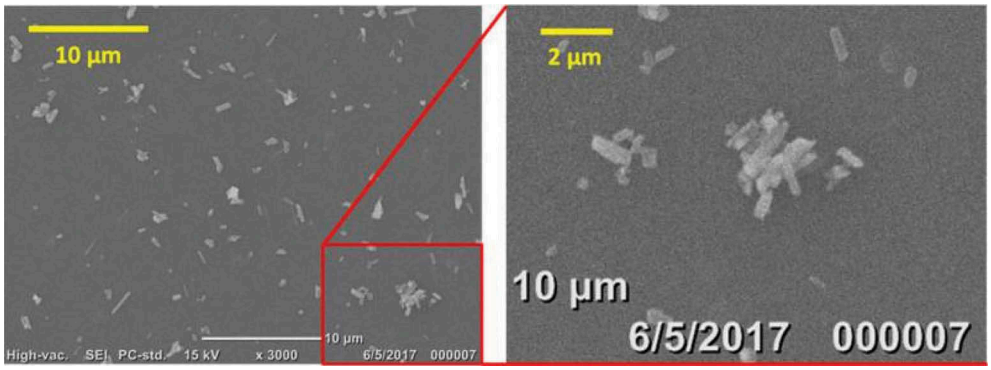

Figure 3. SEM image of the 180-min milled aluminum borate powder (a). The image at left is digital enlargement of the SEM image (b).

C; 540 °C and >1250°C). In order to understand the processes associated with these thermal effects, isothermal stages of the TG-DTA results were observed. For these, the starting powders were fired and air quenched at different temperatures (200, 400, 600 and 1200 °C), labeled Q200, Q400, Q600 and Q1200, respectively, and analyzed by XRD. The XRD patterns are shown in Figure 5, and the identified phases are labeled.

The mass loss below 100°C is around ≈1% wt. (Figure 4) and can be associated with water loss. A small loss can be observed later at which is attributable to some residual boric acid thermal decomposition (≈0.5 wt. %), presumably occurring after the hydration of some active boric oxide from atmospheric humidity or during the ethanol milling treatment. An important mass loss of 2% wt. with the maxima at 540 °C can be detected at T > 470 °C, attributable to the eutectic B_2O_3-$Al_4B_2O_9$ melting at

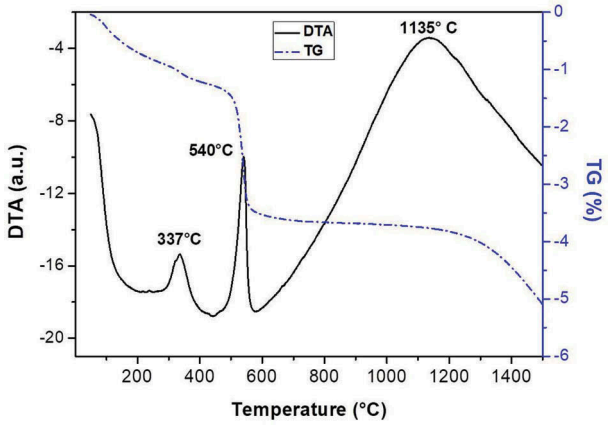

Figure 4. TG-DTA curves of the $Al_{18}B_4O_{33}$ milled powder in an air atmosphere.

449 °C to form a B_2O_3-rich liquid phase, in agreement with Guzalla et al. [30].

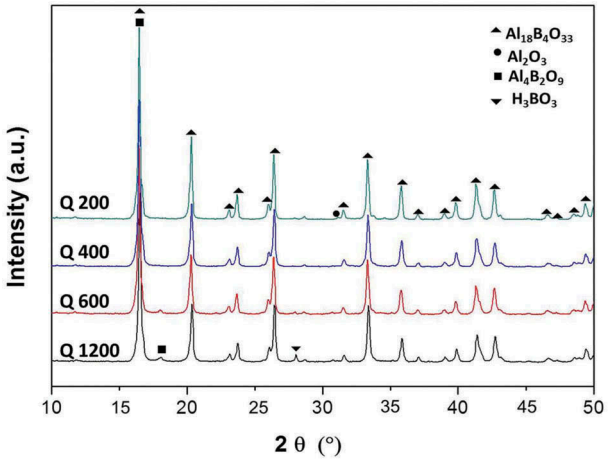

Figure 5. XRD patterns of the isothermally treated (200, 400, 600, 1200 °C; Q200, Q 400, Q600 and Q1200, respectively) and quenched powders.

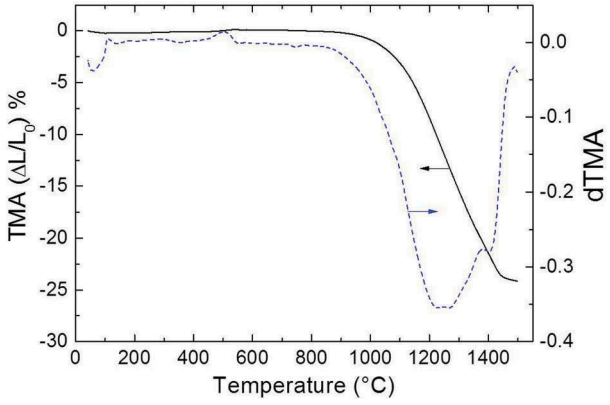

Figure 6. TMA and dTMA curves of the milled powder.

An incongruent melting of a small amount of $Al_4B_2O_9$ into $Al_{18}B_4O_{33}$ and a B_2O_3-rich liquid occurs at 1035°C with a gradual mass loss which starts at T > 1000°C, probably due to the B_2O_3-rich liquid decomposition.

The two intermediate processes (eutectic H_3BO_3 – $Al_4B_2O_9$ fusion and incongruent $Al_4B_2O_9$ melting) are accompanied by exothermic peaks in the DTA curve [31]. The amount of boron oxide loss at 520°C corresponds to an initial $Al_4B_2O_9$ content of approximately 10% in the milled starting powder.

Continuing mass loss was observed at T > 1200°C, suggesting a decomposition reaction. Significant amounts of α-Al2O3 were found in the resulting product indicating the weight loss to be caused by loss of the B_2O_3 gas phase by a vaporization process of the B_2O_3-rich liquid phase. Thermal analysis indicates incongruent melting of the Al-rich aluminum borate phase.

3.3. Evolution of densification, shrinkage and porosity with thermal treatment

Figure 6 shows the shrinkage curve and its derivatives (TMA and dTMA). These clearly show that the powder starts sintering at ≈900°C. It is clearly gradual up to 1200°C and 5% relative shrinkage. Subsequently, a constant shrinkage rate (≈−3.5 10^{-3}/°C) can be observed at between 1200 and 1290°C. The shrinkage rate decreases gradually from ≈−3.5 to −2.7 (10^{-3}/°C) at 1350°C. At this temperature, borate decomposition becomes significant (see Figure 4), and the shrinkage rate remains constant up to 1400°C. The shrinkage stops abruptly at this temperature. This range lacks interest because the decomposition is significant. The borate sintering range must fall below these temperatures.

Finally, a small peak can be observed in the dTMA curve, centered at 540°C. This corresponds to the exothermic DTA peak (Figure 4) associated with the residual $Al_4B_2O_9$ decomposition into $Al_{18}B_4O_{33}$ and B_2O_3 [31].

3.4. Shrinkage and textural evolution. aluminum borate stability as a function of sintering temperature

The sintering behavior was also assessed by batch test. Three disc-shaped samples were fired and analyzed under each set of sintering conditions. Archimedes test results are shown in Table 3.

Figure 7 shows the open porosity (P) and apparent density (D) as functions of the sintering temperature. The achieved sintering grade (P ≈ 10%) is significant especially when compared to the densification attained by the reaction sintering route [27] (P ≈ 45%).

Figure 8 shows the effect of soaking time at 1300°C. An advance of sintering with soaking time is expected for isothermal temperatures. Nevertheless, 10-h treatment presented higher porosities. Apparently, the two processes of sintering and dissociation with boron oxide evaporation occur simultaneously at this temperature. For shorter times, sintering is more significant, causing overall the final effect of densification. But at longer than 5 h, the evaporation gains significance, as observed from the increments of the porosity. In spite of this, the final porosity after 10 h is still lower than that obtained by the reaction sintering route [27], which is also plotted in Figure 8.

The developed crystalline phases of the sintered samples were also studied and are shown in Figures 9 and 10. The only crystalline phase detected is the aluminum borate ($Al_{18}B_4O_{33}$) phase for the samples fired at 1250 and 1300°C soaked for 2 h.

When fired at 1350°C or higher temperatures, $Al_{18}B_4O_{33}$ is accompanied by corundum (Al_2O_3) evidencing a partial or full (1500°C) incongruent

Table 3. Textural properties: apparent density, porosity and qualitative crystalline phase content of the sintered samples. +++ +major, ++abundant, +minor.

Sample name and sintering temp (°C)	Soaking time (h)	Density (g/cm^3)	Open porosity (%)	$Al_{18}B_4O_{33}$	Al_2O_3
1250	2	2.24 ± 0.06	20.53 ± 0.76	++++	-
1300	2	2.33 ± 0.08	17.54 ± 3.74	++++	-
1300	5	2.52 ± 0.02	10.91 ± 1.09	++++	-
1300	10	2.48 ± 0.02	16.52 ± 0.47	++++	+
1350	2	2.42 ± 0.01	13.99 ± 2.30	++	++
1400	2	2.49 ± 0.05	13.10 ± 0.42	-	++++
1500	2	2.59 ± 0.02	14.09 ± 1.20	-	++++

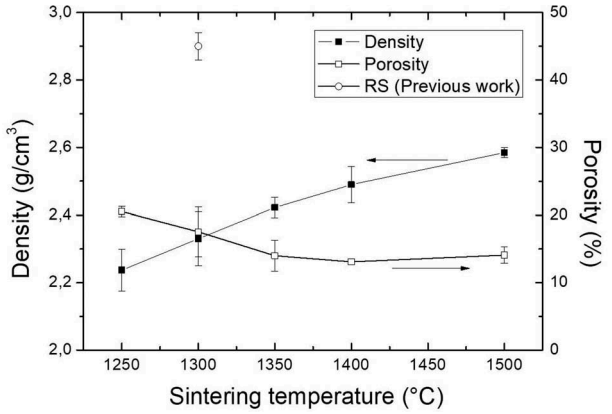

Figure 7. Apparent density and porosity of the sintered materials as functions of sintering temperature with 2 h soaking. RS stands for 'reaction sintered material', and its results are taken from a previous work [27].

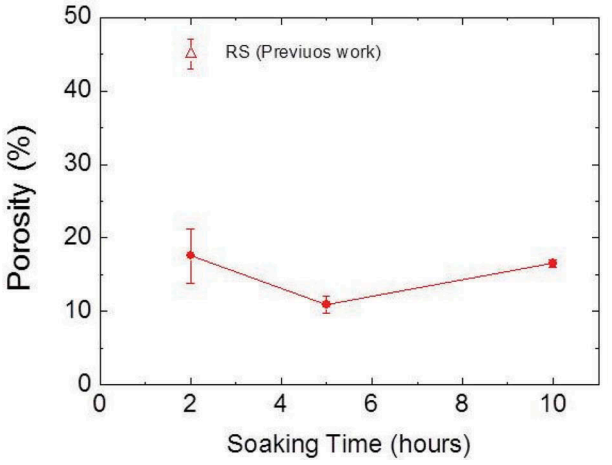

Figure 8. Apparent porosity of the sintered materials at 1300°C as a function of the sintering temperature (bold circles) for different soaking times. RS stands for 'reaction sintered material', and its results are taken from a previous work [27].

decomposition of $Al_{18}B_4O_{33}$ (0.5 $Al_{18}B_4O_{33}$ (s) = 4.5 Al_2O_3(s) +B_2O_3 (g). Thus, the boron oxide is vaporized at these temperatures.

These experiments confirm the decomposition temperature reported by Scholze et al. [32] and previously observed in the TG (Figure 5) and is expected when the Al_2O_3-B_2O_3 phase diagram is taken into account [33].

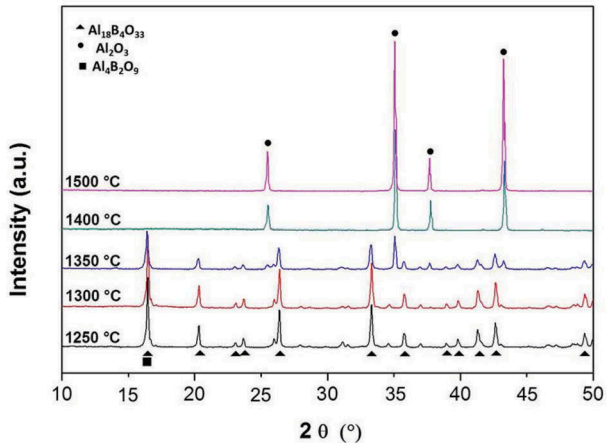

Figure 9. XRD patterns of the sintered samples effect of the sintering temperature with 2 h of soaking.

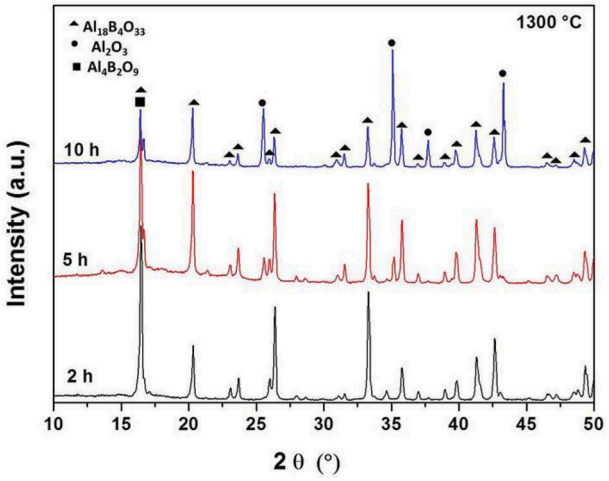

Figure 10. XRD patterns of the sintered samples; effect of the soaking time for borate sintered at 1300°C.

Porosity and density were proportional to the sintering temperature (porosity decreased and density gradually increased with the sintering temperature in the 1200–1350°C range; the sintering study loses at above this temperature interest because the borate thermal decomposition is significant (Figure 9).

The obtained results showed that samples sintered at 1350°C presented partial decomposition and that after processing at higher temperatures the decomposition is almost complete.

The soaking time was then studied for the sample sintered at 1300°C (Figure 10). Very low dissociation

was observed for the 5-h procedure; and dissociation remained became more evident but still low for the 10-h procedure.

The apparent porosity achieved was around 10%, taking into account the fact that the initial compaction grade was 55–60%; in general, the powders were sintered without significant dissociation. The apparent density values were below the theoretical borate specific gravity (2.96 g/cm^3), as expected. This is the first sintering study report on aluminum borate. The shaping processes could be optimized: for example, a higher uniaxial pressure or isostatical press could be employed. Colloidal processing such as slip casting can also be used to improve shaping compaction and enhance the final sinterization processes.

In summary, based on these results the sintering procedure could be optimized, and materials showing higher apparent density were achieved at 1300°C with the 5-h dwelling for both densification and the borate thermal stability.

3.4.1. Resulting microstructures: SEM as a function of sintering temperature

The resulting microstructures encourage the development of future structural applications for these $Al_{18}B_4O_{33}$ materials. Figure 11 shows SEM images of the aluminum borate materials fired at 1300°C with different soaking times: 2, 5 and 10 h. Three magnifications were employed: x500, x5000 and x10000.

In the x500 images homogeneous densification can be observed, and macro-pores (≈5–15 μm) can be identified in the three observed materials. This might result from the inefficient green compaction achieved by the uniaxial press (100 MPa); it could be decreased if a better forming technique were implemented.

The present microstructures consist of dense distributed aluminum borate grains. The sintering processes are advanced. Only some of the grains present the typical rod or whisker morphology [17]. The other grains are angular or sub-angular and present a medium sphericity. The appearance of rod-like grains is lower for the 10-h treatment, showing that during the soaking the rod grains are sintered and transformed in to more rounded grains. Incipient borate decomposition was observed for this material by XRD, revealing that the resultant alumina phase presents a finer grain size (Figure 10). The grains size distribution is larger than the starting grain size (Figure 1), suggesting that with these thermal treatments, the compacted milled powders undergo sinterization accompanied by growth of smaller grains.

The grain size would also affect the mechanical behavior [34]; the observed grain size range is assumed to be similar for the obtained sintered materials (Figure 11), and this fact was taken into account in the mechanical behavior analysis (section 3.4.2).

Finally, the microstructures developed, considered together with the phase evolution during the thermal

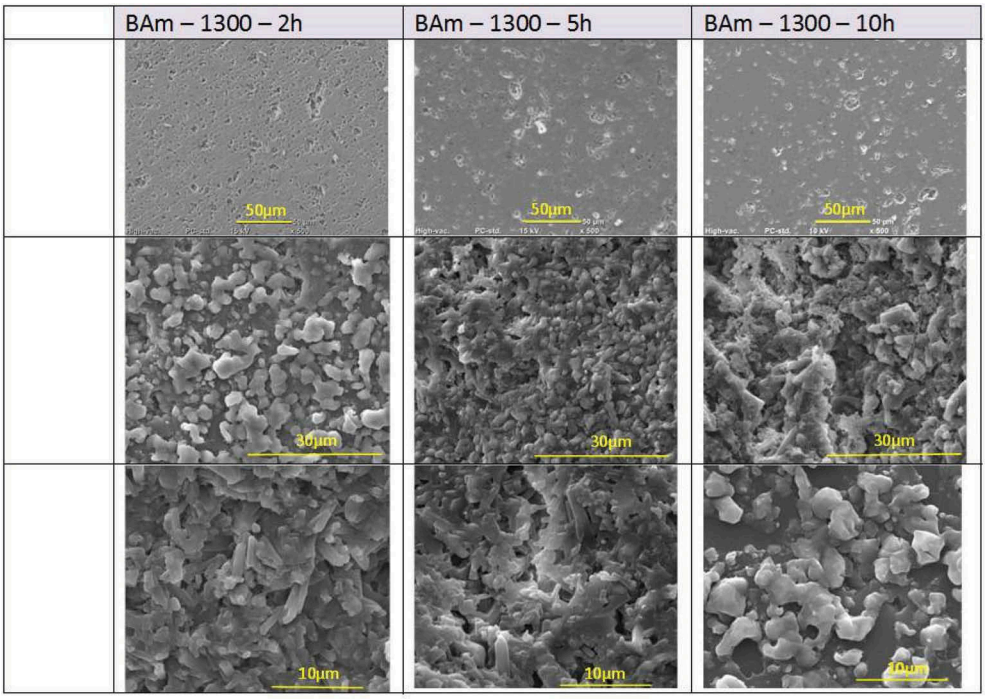

Figure 11. SEM images of $Al_{18}B_4O_{33}$ sintered at 1300°C with different soaking times (2, 5 and 10 h) for the respective columns. Three magnifications (x500, x5000 and x10000) for the respective rows are shown. Polished, etched and gold-coated samples are shown for the x5000 and x10000 images.

treatment of the starting powders, might enlighten the utilization of boron sources as a setting phase for intermediate (800–1200°C) temperature alumina-based and/or spinel-based castables [26]. In such work the boron-alumina phases (different aluminum borates) are proposed as the setting phase for the castables mentioned, which are similar those studied in the present work.

3.4.2. Mechanical properties of the sintered aluminum borate materials, vickers hardness (Hv)

The present work is, to our knowledge, the first bulk hardness report sintered aluminum borate ($Al_{18}B_4O_{33}$). The hardness values of $Al_{18}B_4O_{33}$ wires were measured to be 12.8 GPa [20]. It was found that $Al_{18}B_4O_{33}$ nanowires have higher hardness than $Al_4B_2O_9$ nanowires. It is generally accepted that whiskers exhibit higher stiffness and strength than bulk materials. Their strength is close to the maximum theoretical value derived from the theory of elasticity [5]; this hardness was assumed to be the Hv_0. This is because whiskers are nearly free from internal flaws owing to their small diameters. In this case, the bulk hardness is approximately half that of the reported nanowire hardness; nevertheless, structural applications are encouraged. The porosity effect should also be taken into account; the presence porosity in the developed materials will certainly reduce this property.

Table 4 shows the evaluated Vickers hardness (*Hv*) of the borate materials for different sintering procedures; highly decomposed materials were not evaluated. The achieved hardness values were between 4 and 7 GPa. The uncertainty is below 10% in all cases. The higher evaluated hardnesses correspond to more densified materials. This, together with the developed microstructures, encourages structural application of these materials. The best hardness was achieved for materials fired at 1300 with 5- and 10-h soaking. The former was optimal in terms of densification and thermal decomposition of borate.

MSA model analysis was carried out in order to understand the hardness/porosity/sintering relationships (Figure 12). Different experimental hardness results are plotted together with the exponential relationships. The obtained values are within the 4–7

Table 4. Vickers hardness of the sintered aluminum borate materials and individual wire nano hardness.

Sintering conditions		
Temperature (°C)	Soaking time (h)	Vickers hardness (GPa)
1250	2	4.21 ± 0.41
1300	2	4.53 ± 0.19
1350	2	6.95 ± 0.26
1300	2	4.53 ± 0.19
1300	5	6.12 ± 0.25
1300	10	6.56 ± 0.14
Borate nano hardness [20]		12.8 ± 0.4

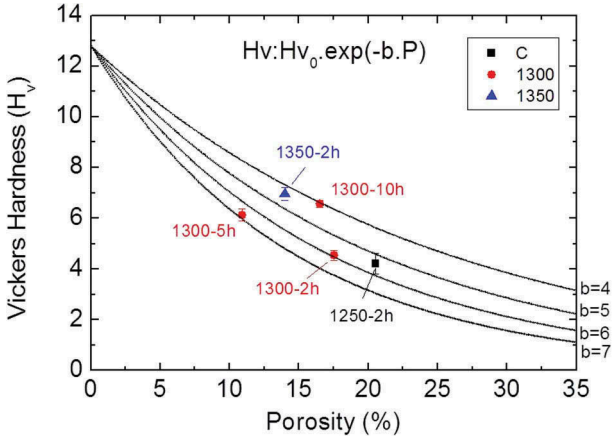

Figure 12. Vickers hardness as a function of open porosity; different corresponding heating procedure are labeled. MSA models are plotted as well (for b parameters b: 4, 5, 6 and 7); the Hv_0 value is the nano hardness: 12.8 GPa [20].

range for the *b* parameter (Table 2). The upper 5 values correspond to polyhedral open pores in solid-sphere stacking structures; the lower 3 correspond to spherical pores. The former are typical under-sintered structures, like the one observed by SEM (Figure 11).

The 1250-2h, 1300-2h and 1300-5h series, particularly correspond to the transition of the b parameter from 5 to 7, which might be understood as a more effective solid-sphere stacking form. On the other hand, 1300-10h and 1350-2h present *b* values of 4 and 4.5, respectively. The corresponding pore structure would be a combination of solid-sphere stacking and spherical pores. This could be associated with the partial decomposition of the borate with boron oxide volatilization that could result in spherical pores around the residual alumina (detected by XRD).

Denser microstructures might present higher hardness, which is wire hardness (12.8 GPa) in all the cases below; a more refined processing route should be carried out for this purpose.

4. Conclusions

Fairly dense aluminum borate ($Al_{18}B_4O_{33}$) materials were obtained by a simple milling-sintering route from aluminum borate powders obtained by thermal reaction of calcined alumina and fine boric acid. The attrition milling was demonstrated to be adequate for milling the initially whisker shape borate powder. An almost complete loss of the whisker-shaped was achieved after 180 min grinding.

The starting milled powder presented some $Al_4B_2O_9$ content (≈10%), which decomposed in to $Al_{18}B_4O_{33}$ and B_2O_3 at low temperature (≈540 °C).

The sintering characteristics of the powder were determined. This starts at around 1000°C and is

limited by the thermal decomposition (T > 1300°C) of the borate to alumina and boron oxide, which volatilize at this temperature. Sub-angular and medium spherical sintered grain microstructures were developed in which some macro-porosity was observed but relatively dense materials were achieved (10% porosity).

The Vickers hardness of ≈6 GPa represents the first hardness report on bulk density aluminum borate material. The values are related to the sintering grade achieved.

The bulk density is below 2.5 g/cm^3, which is low in comparison with other structural materials such as alumina.

The hardness-porosity-sintering relationship was explained in terms of the minimum solid area model; the samples sintered at 1250°C-2h; 1300°C-2h; 1300°C-5h present a solid-sphere stacking form, and, on the other hand, the 1300°C-10h and 1350°C-2h present a combination of solid-sphere stacking and spherical pores.

All the analyses of this system encourage the structural application of borate materials sintered at up to 1300°C. The results also reveal important information on the thermal behavior of the Al_2O_3-B_2O_3 system that is being proposed as a setting (bonding) phase at intermediate temperatures (800–1200°C) of high alumina and/or spinel refractory castables.

Acknowledgments

The authors would like to thank Lic. M.S.Conconi (CETMIC) for the fruitful discussion of XRD results.

Disclosure statement

No potential conflict of interest was reported by the authors.

Funding

The authors would like to thank CONICET and Y-TEC S. A. for their scholarship funding. We are also grateful to CONICET for the international cooperation financial support and ICV Madrid and its staff for receiving us and opening all their facilities for the conduct of this study.

References

[1] Studart AR, Gonzenbach UT, Tervoort E, et al. Processing routes to macroporous ceramics: A review. J Am Ceram Soc. 2006;89:1771–1789.
[2] Ohji T, Fukushima M. Macro-porous ceramics: processing and properties. Int Mater Rev. 2012;57:115–131.
[3] Baudín C. Processing of alumina and corresponding composites. Madrid, Spain: Compr. Hard Mater., Elsevier Ltd., Instituto de Cerámica y Vidrio, CSIC; 2014. 31–72. DOI:10.1016/B978-0-08-096527-7.00021-0.
[4] Ray SP. Preparation and characterization of aluminum borate. J Am Ceram Soc. 1992;75:2605–2609.
[5] Suganuma K, Fujita T, Sasaki G, et al. Evaluation of strength and heat-resistance for aluminum-borate whisker reinforced AC8A aluminum alloy composite. J Jpn Inst Light Met. 1991;41:270–275.
[6] Zhao H, Krysiak Y, Hoffmann K, et al. Elucidating structural order and disorder phenomena in mullite-type Al4B2O9 by automated electron diffraction tomography. J Solid State Chem. 2017;249:114–123.
[7] Hoffmann K, Hooper TJN, Murshed MM, et al. Formation, stability and crystal structure of mullite-type Al6–xBxO9. J Solid State Chem. 2016;243:124–135.
[8] Geng L, Guan LN, Lü K-M. Effects of whisker surface treatment on microstructure and properties of Al18B4O33w/6061Al composites. Trans Nonferrous Met Soc China Engl Ed. 2010;20:349–354.
[9] Peil KP, Galya LG, Marcelin G. Acid and catalytic properties of nonstoichiometric aluminum borates. J Catal. 1989;115:441–451.
[10] El-Hakam SA, El-Sharkawy EA. Structural characterization and catalytic properties of aluminum borates-alumina catalysts. Mater Lett. 1998;36:167–173.
[11] Wang J, Ning G, Yang X, et al. Large-scale synthesis of Al4B2O9/Al18B4O33 whiskers via a novel method. Mater Lett. 2008;62:1208–1211.
[12] Yoshida M, Takeuchi S, Pan J, et al. Preparation and characterization of aluminum borate whisker reinforced magnesium alloy composites by semi-solid process. Adv Compos Mater. 1999;8:259–268.
[13] Cheng C, Ding XX, Shi FJ, et al. Preparation of aluminum borate nanowires. J Cryst Growth. 2004;263:600–604.
[14] Peng LM, Li XK, Li H, et al. Synthesis and microstructural characterization of aluminum borate whiskers. Ceram Int. 2006;32:365–368.
[15] Li Y, Chang RPH. Synthesis and characterization of aluminum borate (Al18B 4O33, Al4B2O9) nanowires and nanotubes. Mater Chem Phys. 2006;97:23–30.
[16] Elssfah EM, Song HS, Tang CC, et al. Synthesis of aluminum borate nanowires via a novel flux method. Mater Chem Phys. 2007;101:499–504.
[17] Peng S, Jinwen H, Wenwei W, et al. Preparation of aluminum borate whiskers by the molten salt synthesis method. Ceram Int. 2013;39:7263–7267.
[18] Gupta RK, Al-Ghamdi AA, Al-Hartomy OA, et al. Synthesis and characterization of nanostructured aluminum borate by sol-gel method. J Sol-Gel Sci Technol. 2012;64:100–103.
[19] Zhou J, Su D, Luo J, et al. Synthesis of aluminum borate nanorods by a low-heating-temperature solid-state precursor method. Mater Res Bull. 2009;44:224–226.
[20] Tao X, Wang X, Li X. Nanomechanical characterization of one-step combustion-synthesized Al 4B2O9 and Al18B4O33 nanowires. Nano Lett. 2007;7:3172–3176.

[21] Fisch M, Armbruster T, Rentsch D, et al. Crystal-chemistry of mullite-type aluminoborates Al18B 4O33 and Al5BO9: A stoichiometry puzzle. J Solid State Chem. 2011;184:70–80.

[22] Luz AP, Santos T Jr., Medeiros J, et al. Sintering additive role on the performance of advanced refractory castables. In: G. D.G., S. J.D., editor. 13th Bienn. Worldw. Congr. Refract. 2013. São Carlos, Brazil: John Wiley and Sons Inc., Federal University of São Carlos, Materials Eng. Dept.; 2014. p. 1099–1104. https://www.scopus.com/inward/record.uri?eid=2-s2.0-85014027075&partnerID=40&md5=b10e8afeb55192addfa90169362afbcd

[23] Luz AP, Silva Neto AB, Santos T, et al. Mullite-based refractory castable engineering for the petrochemical industry, Ceram. Int. 2013;39:9063–9070.

[24] Braulio MAL, Morbioli GG, Pandolfelli VC. Advanced boron-containing Al2O3-MgO refractory castables. J Am Ceram Soc. 2011;94:3467–3472.

[25] Giovannelli Maizo ID, Luz AP, Pagliosa C, et al. Boron sources as sintering additives for alumina-based refractory castables, Ceram. Int. 2017;43:10207–10216.

[26] Hoffmann K, Hooper TJN, Zhao H, et al. Crystal chemical characterization of mullite-type aluminum borate compounds, J. Solid State Chem. 2017;247:173–187.

[27] Hernández MF, Suárez G, Cipollone M, et al. Formation, microstructure and properties of aluminum borate ceramics obtained from alumina and boric acid, Ceram. Int. 2017;43:2188–2195.

[28] Hernández MF, Suárez G, Cipollone M, et al. Mechanical behavior and microstructure of porous needle: aluminum borate (Al18B4O33) and Al2O3-Al18B4O33 composites. Ceram Int. 2017;43:11759–11765.

[29] Rice RW, The porosity dependence of physical properties of materials: A summary review, 1996. https://www.scopus.com/inward/record.uri?eid=2-s2.0-18844402904&partnerID=40&md5=9b7bb95a12760dd7cadfab2ec8abdf76.

[30] Gazulla MF, Gómez MP, Orduña M, et al. Chemical, mineralogical and thermal characterisation of natural and synthetic borates. Boletin Soc Espanola Ceram Vidr. 2005;44:21–31.

[31] Lührs H, Fischer RX, Schneider H. Boron mullite: formation and basic characterization. Mater Res Bull. 2012;47:4031–4042.

[32] Scholze H, Uber Aluminiumborate Z, Anorg F. Allg. Chem. 1956;284:272–277.

[33] Gielisse PJM, Foster WR. The system Al2O3-B2O3. Nature. 1962;195:69–70.

[34] Rice RW, Wu CC, Boichelt F. Hardness–grain-Size relations in ceramics. J Am Ceram Soc. 1994;77:2539–2553.